Physica Scripta. Vol. 70, 368–373, 2004

Effect of Pd Impurity on Charge and Spin Density in Metallic Iron Studied by Mössbauer Spectroscopy

A. Błachowski[1], K. Ruebenbauer[1a] and J. Żukrowski[2]

[1]Mössbauer Spectroscopy Division, Institute of Physics, Pedagogical University, PL-30-084 Cracow, ul. Podchorążych 2, Poland
[2]Solid State Physics Department, Faculty of Physics and Nuclear Techniques, University of Mining and Metallurgy, PL-30-059 Cracow, Al. Mickiewicza 30, Poland

Received January 23, 2004; accepted in revised form June 3, 2004

PACS numbers: 71.20.Be, 75.50.Bb, 76.80.+y

Abstract

Random iron-palladium alloys of BCC structure and containing up to 10.59 at.% of Pd have been investigated by means of 14.4 keV Mössbauer spectroscopy in ^{57}Fe at ambient temperature versus Pd concentration. It has been found that the perturbation of the iron hyperfine field caused by Pd impurity extends to the third co-ordination shell around an iron atom. Perturbations caused by single Pd atom located in the first, second and third co-ordination shell, respectively, were determined. It was found that they depend very weakly on the average Pd concentration in the range of concentrations investigated. On the other hand, similar perturbations of the isomer shift extend to greater distances from the impurity. Individual contributions due to Pd impurity in the first, second and third shell, respectively, are seen up to about 5 at.% of Pd. However they are small compared to the change of the average isomer shift due to more distant impurities. One sees the change of the average shift solely for alloys having higher concentration of Pd than 5 at.%. On the other hand, a contribution to the hyperfine field remains constant beyond the third shell at all Pd concentrations investigated. It is the same as the field in pure iron.

1. Introduction

Mössbauer spectroscopy is sensitive to the electron charge density on the resonant nuclei via isomer shift, and it is simultaneously sensitive to the electron spin density on the resonant nuclei via dipolar magnetic hyperfine interaction provided the sample remains magnetically ordered. Hence one can look at charge and spin density modifications due to charge and spin transfer from adjacent atoms surrounding the resonant atom. If one collects data at relatively low temperature of the sample investigated, i.e., well below the magnetic ordering temperature, one looks approximately at the properties of the ground electronic state of the system. Conduction electrons play a dominant role in the charge and spin transfer in metallic systems. A particularly simple situation is achieved in a ferromagnetic host composed of rather localised atomic magnetic moments provided resonant atoms are one of the host isotopes distributed randomly between other non-resonant host atoms. Such situation occurs in BCC iron.

In order to gain some information about the range of the charge and spin transfer between atoms one can introduce some non-magnetic impurity distributed at random in the host. Low concentrations of impurities are essential to avoid interactions between them. Investigation of several samples with varying concentration of impurities allows for better insight into the problem. An impurity affects charge and spin densities of the conduction electrons, and these perturbations have impact on the observed isomer shift and hyperfine magnetic field. In the case of very long distance perturbations one sees the change of the average shift and field solely. Otherwise a distribution of shifts and fields builds up with increasing concentration of diluted impurities due to various possible configurations around the resonant atom [1].

Iron-palladium alloys have already been investigated [2–5]. However no systematic investigation of alloys rich in iron has been performed up to now. We report here results, obtained for BCC iron doped with palladium in the concentration range extending from pure iron till alloy containing 10.59 at.% of palladium. The paper is organised as follows: section 2. describes experimental procedures applied, section 3. is devoted to the data evaluation, while the last section 4. contains discussion of results and conclusions.

2. Experimental

Samples were prepared by arc melting under argon atmosphere appropriate amounts of natural iron and palladium. Iron ingots of 99.97+ % purity were obtained from Alfa Aesar. Palladium was obtained in form of sheets having purity 99.9%. All samples were melted three times and rapidly cooled. Composition and homogeneity of each sample was checked with the help of electron micro-probe and results are shown in Table I. Mössbauer samples were prepared by powdering of the appropriate ingots with the help of diamond file. The resulting powder was mixed with epoxy resin and absorbers in the form of discs having 26 mm diameter were made subsequently. Approximately 30 mg/cm^2 of iron was used, while preparing absorbers. Spectra were collected at ambient temperature using commercial ^{57}Co(Rh) source having 6 μm thickness and covered by high purity beryllium window of 0.5 mm thickness. The source was purchased from Ritverc G.m.b.H. A Kr/isopenthane filled proportional detector equipped with high purity beryllium window of 0.3 mm thickness was used to collect data. The maximum total count rate was kept low enough to assure linear response of the detector. Mössbauer data were collected in a double ramp round-corner linear velocity mode in 4096 channels using a MsAa-1 spectrometer [6]. Natural iron foil of high purity was used to calibrate the velocity scale. Raw data were folded and subsequently the content of each two adjacent channels was added to improve the statistical accuracy. Such a procedure resulted in 1023 data points per each spectrum collected. Background under resonant γ-ray line of 14.4 keV was measured prior and after collecting each Mössbauer spectrum.

3. Data evaluation

Mössbauer data were evaluated applying MOSGRAF Mössbauer data evaluation software system [7, 8]. A transmission integral approximation in the resonantly thin source limit was used [9].

[a]Corresponding author: Electronic address: sfrueben@cyf-kr.edu.pl
World Wide Web: www.cyf-kr.edu.pl/~sfrueben/

Table I. *Concentration of palladium determined by the electron micro-probe.*

Sample	0	1	2	3	4	5	6
c [at.%]	0	0.95 ± 0.03	2.76 ± 0.06	4.71 ± 0.07	6.63 ± 0.05	8.04 ± 0.09	10.59 ± 0.10

Essential source parameters like source line width and effective source recoilless fraction were derived from the spectrum of the above mentioned velocity calibration iron foil. The average background under the γ-ray line of each spectrum was used to calculate a specific effective source recoilless fraction applicable to this particular spectrum. The natural assumption that the source emits a single unpolarised line was used throughout the data evaluation procedure. The average absorber dimensionless resonant thickness was treated as adjustable parameter for each data set. All line widths within the absorber were constrained to the same, albeit adjustable, value for each sub-spectrum line analysed. Furthermore, they were constrained to be the same for outermost, intermediate and innermost pairs of lines. This procedure allowed sufficient correction for slight radiation beam divergence. It was found that the electric quadrupole interaction is below detection threshold in all spectra collected. On the other hand, some distribution of the semi-classical time independent magnetic dipole interactions is seen as expected for the ferromagnetic samples well below the magnetic transition temperature. A correlated distribution of the total spectral shift is seen as well. It is believed that the latter distribution is due entirely to the scatter in the isomer shift, as the second order Doppler shift is characterised well by a single value due to the fact, that ambient temperature is high enough to obey satisfactorily the Dulong-Petit rule [10]. Some slight magnetisation of the samples in the sample plane, i.e., perpendicular to the weakly divergent beam of radiation is observed, and it has been accounted for allowing to vary the dipolar diagonal anisotropy coefficient set as common for all sub-spectra of the given data set [11]. Such a magnetisation has negligible effect on hyperfine magnetic fields. A distribution of the hyperfine magnetic field and correlated distribution of the isomer shift has been analysed under the assumption that non-magnetic palladium atoms are distributed randomly within the BCC host lattice of iron. It has been assumed that the recoilless fractions are the same for all encountered configurations, and that they are isotropic. Furthermore, it was assumed that effects caused by impurities are strictly additive and isotropic. In such a case one can add contributions resulting from equivalent configurations, and to obtain a relative contribution from a particular non-equivalent configuration in accordance with the binomial distribution law provided identity of particular shells is maintained despite alloying in impurities [1]. Such a contribution can be expressed as follows:

$$C_\sigma(c|\{n_s k_s\}) = \prod_{s=1}^{\sigma} \left[\left(\frac{n_s!}{(n_s - k_s)! k_s!} \right) c^{k_s} (1-c)^{n_s - k_s} \right]. \tag{1}$$

The symbol $0 < c < 1$ denotes atomic concentration of palladium impurities determined from the electron micro-probe results. The index $s = 1, 2, \ldots, \sigma$ enumerates subsequent co-ordination shells around the central resonant iron atom with $\sigma \geq 1$ being the index of the outermost shell taken into consideration. Finally, the symbol $n_s \geq 1$ denotes the number of vortices in the shell s, and the index $k_s = 0, 1, \ldots, n_s$ enumerates the number of impurities in the shell s for a particular non-equivalent configuration. Numbers n_s are available readily from the known crystal lattice topology. The symbol $\{n_s k_s\}$ denotes a particular set of the indices n_s and k_s, the latter applying to a particular configuration having the contribution $C_\sigma(c|\{n_s k_s\})$. The above contributions are positive and normalised to unity, i.e. the following relationship is obeyed:

$$\sum_{s=1}^{\sigma} \sum_{k_s=0}^{n_s} C_\sigma(c|\{n_s k_s\}) = 1. \tag{2}$$

Particular hyperfine fields and isomer shifts are obtained respectively in the following way:

$$B_\sigma(\{n_s k_s\}) = B_0^{(\sigma)} + \sum_{s=1}^{\sigma} k_s \Delta B_s$$

and

$$S_\sigma(\{n_s k_s\}) = S_0^{(\sigma)} + \sum_{s=1}^{\sigma} k_s \Delta S_s. \tag{3}$$

Here symbols $B_0^{(\sigma)}$ and $S_0^{(\sigma)}$ denote field and total shift, respectively for resonant atoms surrounded entirely by iron atoms up to the outermost shell σ inclusive. On the other hand, symbols ΔB_s and ΔS_s denote respective contributions to the field and isomer shift due to a single palladium atom located in the shell s instead of the iron atom. The above mentioned parameters were treated as variables, while processing data. The last variable for each data set was the number of counts far off resonance. Data were analysed either setting $\sigma = 2$ or $\sigma = 3$. It is worth noticing that for the BCC lattice encountered here one obtains $n_1 = 8, n_2 = 6$ and $n_3 = 12$. Essential results are shown in Tables II and III. Folded spectra are shown in Figure 1.

The average hyperfine field and average total shift can be calculated according to the following relationships, respectively:

$$\begin{aligned} \langle B \rangle_\sigma &= \sum_{s=1}^{\sigma} \sum_{k_s=0}^{n_s} C_\sigma(c|\{n_s k_s\}) B_\sigma(\{n_s k_s\}) = B_0^{(\sigma)} + c \sum_{s=1}^{\sigma} n_s \Delta B_s, \\ \langle S \rangle_\sigma &= \sum_{s=1}^{\sigma} \sum_{k_s=0}^{n_s} C_\sigma(c|\{n_s k_s\}) S_\sigma(\{n_s k_s\}) = S_0^{(\sigma)} + c \sum_{s=1}^{\sigma} n_s \Delta B_s. \end{aligned} \tag{4}$$

Table II. *Essential results obtained within binomial distribution model with $\sigma = 2$. The last row shows the averages of respective columns, where appropriate.*

c [at.%]	$\langle B \rangle_2$ [T] ± 0.02	$B_0^{(2)}$ [T] ± 0.02	ΔB_1 [T] ± 0.02	ΔB_2 [T] ± 0.02	$\langle S \rangle_2$ [mm/s] ± 0.002	$S_0^{(2)}$ [mm/s] ± 0.002	ΔS_1 [mm/s] ± 0.002	ΔS_2 [mm/s] ± 0.002
0	32.97				0			
0.95	33.17	33.03	1.20	0.51	0.008	0.006	0.014	0.007
2.76	33.53	33.22	1.19	0.90	0.023	0.019	0.015	0.011
4.71	32.87	33.28	1.08	0.98	0.036	0.028	0.019	0.005
6.63	34.23	33.34	1.26	0.76	0.048	0.044	0.006	0.001
8.04	34.48	33.39	1.28	0.86	0.057	0.054	0.003	0.002
10.59	34.70	33.50	1.09	0.71	0.064	0.061	0.003	0.003
			1.18	**0.79**				

Table III. *Essential results obtained within binomial distribution model with $\sigma = 3$. The last row shows the averages of respective columns, where appropriate.*

c [at. %]	$\langle B\rangle_3$ [T] ±0.02	$B_0^{(3)}$ [T] ±0.02	ΔB_1 [T] ±0.02	ΔB_2 [T] ±0.02	ΔB_3 [T] ±0.02	$\langle S\rangle_3$ [mm/s] ±0.002	$S_0^{(3)}$ [mm/s] ±0.002	ΔS_1 [mm/s] ±0.002	ΔS_2 [mm/s] ±0.002	ΔS_3 [mm/s] ±0.002
0	32.97					0				
0.95	33.18	32.96	1.66	0.95	0.61	0.008	0.006	0.015	0.011	0.006
2.76	33.55	33.07	1.28	1.05	0.68	0.023	0.018	0.015	0.011	0.005
4.71	33.87	33.17	1.39	0.97	0.38	0.035	0.026	0.018	0.014	0.004
6.63	34.20	32.86	1.41	0.97	0.92	0.045	0.042	0.004	0.003	0.001
8.04	34.50	33.00	1.37	1.14	0.85	0.052	0.047	0.007	0.004	0.001
10.59	34.67	32.98	1.16	1.19	0.58	0.065	0.061	0.003	0.003	0.002
		33.01	**1.38**	**1.05**	**0.67**					

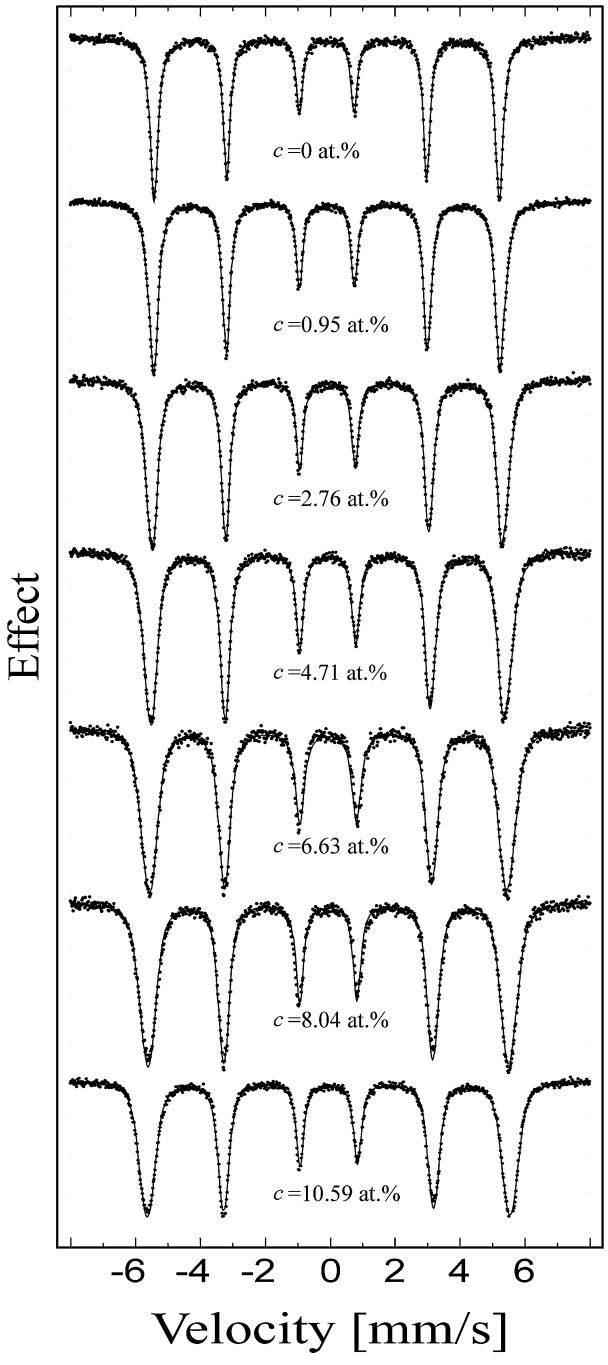

Fig. 1. Mössbauer spectra obtained for alloys investigated. Solid lines correspond to binomial distribution data evaluation method with $\sigma = 3$. Vertical scale is not shown in detail as count statistics and sample thickness varied from case to case.

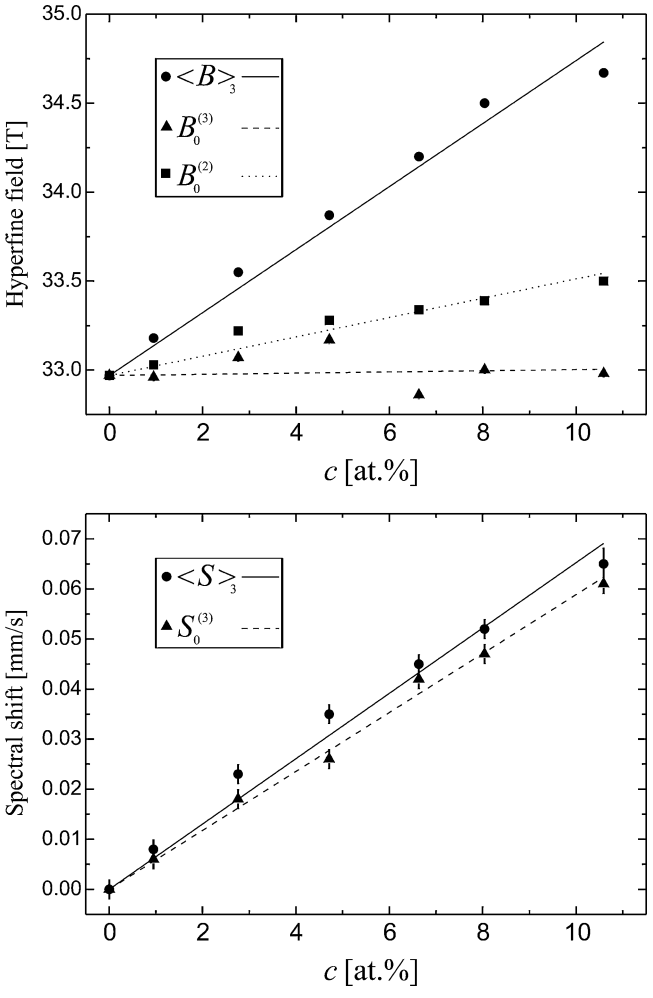

Fig. 2. Hyperfine field and relative spectral shift plotted versus palladium concentration. Straight lines are the lowest order approximations to the trends observed, particularly for shifts.

The average field and shift for the case $\sigma = 3$ are plotted versus palladium concentration c in Figure 2 together with parameters $B_0^{(3)}$ and $S_0^{(3)}$. A plot of $B_0^{(2)}$ versus c is added for comparison as well. It is clearly seen that $\left(\frac{\partial B_0^{(3)}}{\partial c}\right) \approx 0$, while $\left(\frac{\partial S_0^{(3)}}{\partial c}\right) > 0$. Spectral shifts reported in this paper refer to the total shift of metallic iron kept in the vicinity of room temperature. It should be noted that parameters ΔB_s and ΔS_s depend to some extend on palladium concentration c and the number of shells σ taken into account. Such behaviour is understandable due to the fact that the formalism outlined above is some approximation to a more

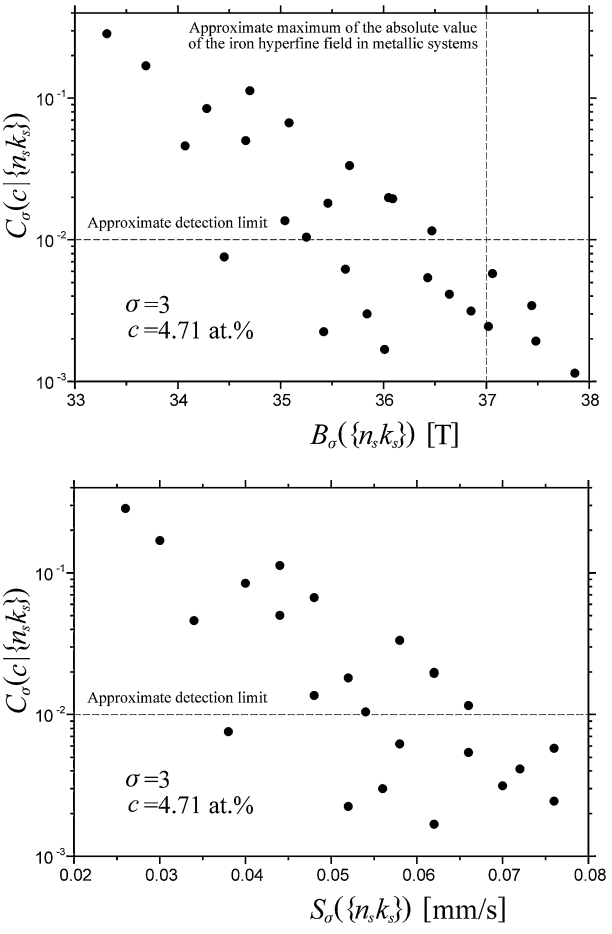

Fig. 3. Binomial distribution of hyperfine field and isomer shift plotted for one of the palladium concentrations investigated.

complex reality. Overall experimental spectral shifts are rather small, as both source and absorber are metallic systems.

The above formalism is restricted of course to low non-magnetic impurity concentrations, as otherwise interactions between impurities cannot be neglected. However at low concentrations configurations rich in impurities have insignificant impact on the spectra shape. A distribution of the hyperfine field and spectral shift above outlined is described by $2\sigma + 3$ parameters at most provided the concentration of impurities c is treated as variable. Otherwise the maximum number of variables describing distribution equals $2(\sigma + 1)$.

Figure 3 shows distributions of hyperfine field and total shift encountered in some of the samples investigated. Contributions from sub-spectra having relative intensities less than 0.1% are not shown. Some minor and thus irrelevant contributions resulting from very high fields or shifts are not shown as well. It has to be remembered that the sign of the hyperfine field has no effect on the spectra in the absence of strong external magnetic field. This statement applies to spectra recorded during this investigation. Finally, it should be understood that the statement sub-spectrum applies rather to the partial absorption cross-section than to the real sub-spectrum, as the data were evaluated using a transmission integral formalism.

A correlation between hyperfine field and isomer shift distributions is clearly seen in the spectrum of the sample with $c = 4.71$ at.% as the asymmetry in the amplitudes of the second and fifth dip (see, Figure 1).

All data were independently evaluated using modified Hesse-Rübartsch formalism [12, 13]. A distribution of the hyperfine field was derived in the thin absorber limit keeping common and constant the line width for each pair of lines in each sextet, and common and constant shift for all sextets. It was assumed that the sample has completely random orientation of the hyperfine fields. The number of counts far off resonance was adjusted for each spectrum as well. Line widths were estimated using known source line width, each absorber dimensionless resonant thickness and appropriate absorber line widths obtained by the previous method in the $\sigma = 3$ limit. A correction to each line width due to the absorber thickness was applied here in the linear approximation limit. A total shift was calculated as the average over the absorption profile for each data set applying known velocity scale of each data set, and estimation of the number of counts far off resonance based on the spectral wings of each data set. The hyperfine field scale was set to the range 29.90–38.10T divided into 40 equal intervals. Resulting distributions normalised to unity are shown in Figure 4, while the average fields $\langle B \rangle$ and shifts relative to metallic iron at room temperature $\langle S \rangle$ are shown in Table IV. Contributions less than or approximately equal to 1% are not shown. A distribution obtained for pure iron represents a resolution of the method. It is interesting to note that the average fields obtained this way are practically the same as resulting from the binomial distribution. On the other hand, shapes of the Hesse-Rübartsch distributions are vastly different from the shapes of the corresponding binomial distributions. Hence higher than the first moment are not reproduced reliably by the Hesse-Rübartsch method for these relatively narrow distributions despite quite good reproduction of the spectra shape. On the other hand, average shifts obtained by all three methods applied are practically

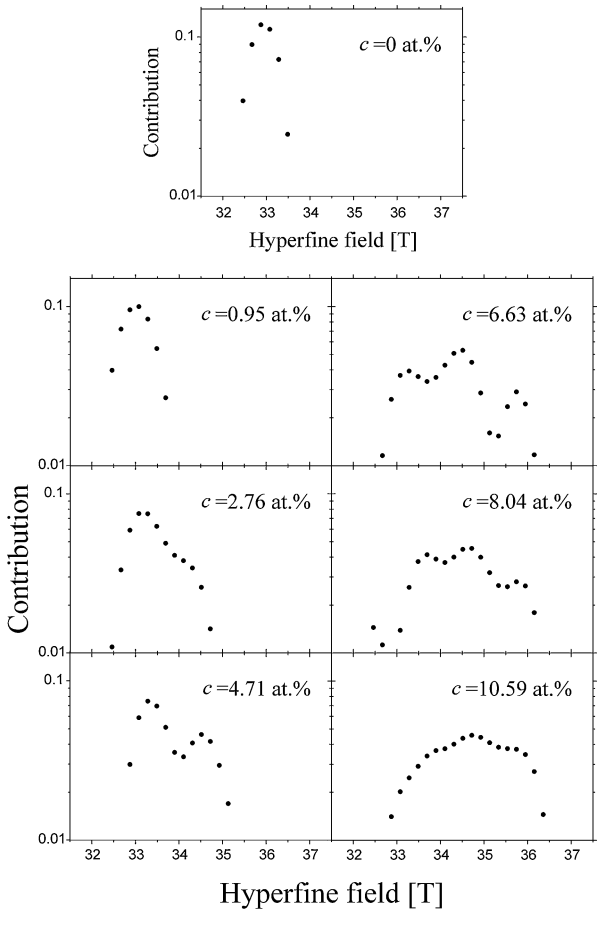

Fig. 4. Distributions of the hyperfine field obtained by the Hesse-Rübartsch method.

Table IV. *Average hyperfine field and relative spectral shift obtained applying Hesse-Rübartsch method.*

c [at. %]	$\langle B \rangle$ [T] $\pm$ 0.02	$\langle S \rangle$ [mm/s] $\pm$0.002
0	32.99	0
0.95	33.18	0.009
2.76	33.56	0.023
4.71	33.88	0.035
6.63	34.25	0.045
8.04	34.52	0.056
10.59	34.64	0.065

the same for all samples. Figure 4 shows distributions obtained with the smoothing parameter [12, 13] set to unity, i.e., close to the optimum. However comparable quality fits can be obtained with very large values of the smoothing parameter. Distributions obtained in the latter case have distinctly different shapes than those of Figure 4, particularly for larger palladium concentrations.

4. Discussion and conclusions

One has to note that the hyperfine magnetic field at iron nucleus is mainly caused by the Fermi contact term proportional to the spin electron density at the nucleus. A spin density is predominantly due to electrons of s-type, as iron is not a particularly heavy element. On the other hand, an almost constant spin density within the nucleus can be in principle split into an atomic part and a part transferred from the adjacent magnetic atoms. The latter contribution is transferred via conduction electrons in the case of metallic systems. These two contributions to the hyperfine field can be added algebraically for a ferromagnetic system having fairly isotropic Fermi surface [14–16]. It has to be noted that they have opposite signs in the case of iron atom embedded in BCC metallic iron. Hence the increase of the field upon alloying with palladium is an indication that the overall transferred spin density diminishes on iron with alloying in palladium. Another important point is that the field within a cluster containing solely iron to the third co-ordination shell inclusive is almost independent of the palladium concentration, and nearly the same as in pure iron. Hence the spin density perturbation on the iron nucleus due to the palladium impurity vanishes at distances larger than approximately $\sqrt{2}a$, where a stands for the average lattice constant of the chemical unit cell. The above interaction length seems to be independent of the palladium concentration at least for relatively low concentrations. Therefore it is rather a property of pure iron. Similar results were found investigating pure mono atomic layers of ^{57}Fe deposited on the surface of single crystal of ^{56}Fe and covered subsequently by some layers of ^{56}Fe again. A third layer beneath the sample surface exhibits practically the same field as bulk iron. On the other hand, the electric field gradient vanishes beyond the second layer [17]. Hence one cannot expect any discernible electric field gradient upon alloying with the element exhibiting high electron charge density in comparison with vacuum. Our values of ΔB_1 are similar to the value obtained by Vincze and Campbell [2] provided data are evaluated setting $\sigma = 2$. The agreement between our values of ΔB_2 and their corresponding value is less satisfactory, albeit still fair provided our data are evaluated within the $\sigma = 2$ model again. It is believed that dipolar magnetic fields generated by adjacent palladium impurities are negligible, as palladium exhibits very large magnetic susceptibility in metallic environment.

The isomer shift is proportional to the electron charge density at the nucleus. The isomer shift increases with decreasing electron density for the nuclear transition used in this study. Hence one can conclude that the overall electron density at the iron nucleus decreases with adding palladium to the alloy. However the evolution of the electron density behaves differently than the evolution of the spin density with increasing concentration of palladium. First of all long range, i.e., conduction band effects are dominant as the isomer shift within the centre of the above mentioned cluster follows the palladium concentration. Effects due to palladium atoms in the third shell are almost negligible, while contributions due to impurities in the first and second shell become irrelevant at palladium concentration exceeding about 5 at.%, i.e., an approximate solubility limit of palladium in BCC iron close to the BCC-FCC transition temperature in pure iron [18]. Each discernible palladium impurity reduces simultaneously electron density and electron spin density on the iron nucleus.

It has been confirmed that neither charge density nor spin density perturbation seen by the iron nucleus and due to the palladium impurity has oscillatory character, and that all contributions due to the above impurity have respectively the same sign. Such behaviour was found earlier [2] by other researchers. The lack of spin density oscillations could be understood remembering that the system contains a lot of rather localised atomic magnetic moments ordered in ferromagnetic fashion. A small magnetic moment has been attributed to palladium atom in alloys considered [4], however it is likely that it is due to the enhanced spin polarisation of the conduction band in the vicinity of the palladium impurity.

In conclusion one can make a statement that electrons responsible for magnetic moment transfer are much more localised in the system investigated than electrons responsible for charge transfer. The electric charge is transferred more or less directly by means of the conduction electrons of s-type, while the local spin density is influenced mainly by local exchange interactions with d-type conduction electrons carrying a dominant contribution to the spin-like magnetic moment. In other words, it seems that few electronic eigenstates of the particular wave number contribute coherently to the charge transfer, while many such states contribute to the spin transfer within the conduction band involved. Therefore perturbations caused by the impurity have different ranges for charge and spin transfer, respectively.

One has to be cautious while trying to interpret higher moments of the hyperfine magnetic field distribution obtained by some model independent method [12, 13] particularly for narrow distributions, as distributions obtained this way may have quite artificial shapes.

Birsan *et al*. [4] attempted recently to introduce a consistent model describing hyperfine field distribution on iron nuclei and magnetisation data for iron-palladium BCC alloys. This model was based on calculations performed previously by Drittler *et al*. [19]. They found non-vanishing contributions to the hyperfine field caused by palladium impurity up to the fifth co-ordination shell. However the last model seems to predict significant contributions due to unrealistically large fields. Distributions were not fitted to the experimental data like in this article, but calculated *ex post*. They applied Le Caër and Dubois method [13] to their data as well, but it seems that their hyperfine field interval was too coarse. The isomer shift distribution was not

taken into account, but its imprint on the Mössbauer data can be seen in the spectra shown by them. Their samples were prepared applying mechanical alloying method, and hence they might be different from ours due to the high concentration of defects introduced by the method of mechanical alloying. However the basic results of the paper [4] are in good agreement with the present results. The average field obtained experimentally agrees quite well with our results in the common region of the palladium concentration investigated. Hence it seems essential to perform some *ab initio* calculations of the electronic structure in the iron-palladium system in order to get rid of the dubious assumptions concerned with the arbitrary division of electrons into core and band electrons. The best currently available results of *ab initio* calculations cannot be readily applied [5], as they were restricted to four atoms in the chemically ordered structure. They predict actually the increased iron magnetic moment with the increasing concentration of palladium in accordance with the Mössbauer results. However this effect is overestimated in comparison with the experimental data provided the scaling law applies between the magnetic moment and the hyperfine field, as no direct calculations of the iron hyperfine magnetic fields were performed [5]. The scaling law might be questionable as calculated iron magnetic moments [5] reproduce experimentally determined iron moments quite well [4].

Cheng *et al*. [20] performed recently conversion electron Mössbauer measurements on thin layers composed of iron and palladium. Their results cannot be directly compared with the results obtained using alloys due to the significant modification of the conduction band in almost two-dimensional systems. However they found very similar behaviour of the isomer shift and hyperfine field seen by the iron nucleus in the vicinity of the palladium impurities. They found that the perturbation to the iron hyperfine field practically disappears beyond the second iron atomic layer from the interface between palladium and iron layers. The last result is in good agreement with our observation that no perturbation is seen beyond third neighbours.

References

1. Zemčik, T., "Proceedings International Conference on Mössbauer Spectroscopy". (Edited by A. Z. Hrynkiewicz and J. A. Sawicki) (Cracow 1975), vol. II, p. 59.
2. Vincze, I. and Campbell, I. A., J. Phys. F: Metal Phys. **3**, 647 (1973).
3. Klimars, S., Hesse, J. and Huck, B., J. Magn. Magn. Mat. **51**, 183 (1985).
4. Birsan, M., Fultz, B. and Anthony, L., Phys. Rev. B **55**, 11502 (1997).
5. Shi, Y. S., Qian, D., Dong, G. S., Jin, X. F. and Wang, D. S., Phys. Rev. B **65**, 172410 (2002).
6. Kwater, M., *et al*., Acta Physica Slovaca **45**, 81 (1995).
7. Ruebenbauer, K. and Birchall, T., Hyperfine Interact. **7**, 125 (1979).
8. Ruebenbauer, K., "^{119}Sn Mössbauer Spectroscopy in the Magnetically Diluted Heusler-type Systems". (Institute of Nuclear Physics, Cracow 1981), p. 127; see also: www.cyf-kr.edu.pl/∼sfrueben/
9. Margulies, S., Debrunner, P. D. and Frauenfelder, H., Nucl. Instrum. Meth. **21**, 217 (1963).
10. Sepioł, B., Ruebenbauer, K., Miczko, B. and Birchall, T., Physica B **168**, 159 (1991).
11. Ruebenbauer, K., Physica B **172**, 346 (1991).
12. Hesse, J. and Rübartsch, A., J. Phys. E: Sci. Instrum. **7**, 526 (1974).
13. Le Caër, G. and Dubois, J. M., J. Phys. E: Sci. Instrum. **12**, 1083 (1979).
14. Watson, R. E. and Freeman, A. J., Phys. Rev. **123**, 2027 (1961).
15. Ofer, S., Nowik, I. and Cohen, S., "Chemical Applications of the Mössbauer Spectroscopy". (Edited by V. I. Goldanskii and R. H. Herber) (Academic Press, New York and London 1968).
16. Friedt, J. M. and Sanchez, J. P., J. Phys. C: Sol. State Phys. **11**, 3731 (1978).
17. Korecki, J. and Gradmann, U., Phys. Rev. Lett. **55**, 2491 (1985).
18. Massalski, T. B., "Binary Alloy Phase Diagrams". (ASM International, Materials Park, Ohio 1990), vol. II, p. 1751.
19. Drittler, B., Stefanou, N., Blugel, S., Zeller, R. and Dederichs, P. H., Phys. Rev. B **40**, 8203 (1989).
20. Cheng, L., Altounian, Z., Ryan, D. H. and Ström-Olsen, J. O., J. Appl. Phys. **91**, 7188 (2002).

